Excess Electron Relaxation Dynamics at Water/Air Interfaces

Ádám Madarász

Eötvös Loránd University, Department of Physical Chemistry, Budapest 112, P. O. Box 32, H-1518, Hungary

Peter J. Rossky[1]

Department of Chemistry and Biochemistry, Institute for Theoretical Chemistry, University of Texas at Austin, Austin, TX 78712-1167

László Turi[2]

Eötvös Loránd University, Department of Physical Chemistry, Budapest 112, P. O. Box 32, H-1518, Hungary

We have performed mixed quantum-classical molecular dynamics simulations of the relaxation of a ground state excess electron at interfaces of different phases of water with air. The investigated systems included ambient water/air, supercooled water/air, *Ih* ice/air and an amorphous solid water/air interfaces. The present work explores the possible connections of the examined interfacial systems to finite size cluster anions, and the three-dimensional infinite, fully hydrated electron.

[1] E-mail: rossky@mail.utexas.edu, fax: (1)-512-471-3555.

[2] E-mail: turi@chem.elte.hu, fax: (36)-1-372-2592.

Localization site analyses indicate that in the absence of nuclear relaxation the electron localizes in a shallow potential trap on the interface in all examined systems in a diffuse, surface-bound (SB) state. With relaxation, the weakly bound electron undergoes an ultrafast localization and stabilization on the surface with the concomitant collapse of its radius. In the case of the ambient liquid interface the electron slowly (on the 10 ps timescale) diffuses into the bulk to form an interior-bound (IB) state. In each other case, the excess electron persists on the interface in surface-bound (SB) states. The relaxation dynamics occur through distinct SB structures which are easily distinguishable by their energetics, geometries, and interactions with the surrounding water bath. The systems exhibiting the most stable SB excess electron states (supercooled water/air and *Ih* ice/air interfaces) are identified by their characteristic hydrogen-bonding motifs which are found to contain double acceptor type water molecules in the close vicinity of the electron. These surface states correlate reasonably with those extrapolated to infinite size from simulated water cluster anions.

I. Introduction

The presence of charged species at interfaces plays a key role in a wide range of physical processes. Heterogeneous charge transfer is among the most notable examples with implications in electrochemistry, atmospheric chemistry, heterogeneous catalysis, or from a more general viewpoint, in through-space electron transfer reactions taking place in biological systems. Additional important examples have been reviewed recently in connection with electron-initiated processes in aqueous systems.[1]

An excess electron at a water/air interface may be considered as a model system in this class, and a number of experimental efforts of such systems are appearing in the recent literature (see Ref. 2). Excess electrons are known to stabilize in bulk aqueous systems, as hydrated electrons.[3] Since the first experimental identification of the species,[4] the hydrated electron has drawn significant scientific attention both experimentally[5,6,7,8,9,10,11] and theoretically.[12,13,14,15,16,17,18,19,20] According to the widely accepted picture, the hydrated electron occupies a solvent void, [5,14] and its behavior resembles that of a particle in a spherical box, although the electron is self-trapped producing an electronic polarization in the solvent. The ground state of the excess electron can be characterized by an approximately spherical wave function, followed in energy by three quasi-degenerate *p*-type excited states.[14] The basic reason for the utility of this simple picture is that water molecules have stable, closed electron shells, so that the excess electron can be treated more or less separately from the other electrons in the system. Ab initio calculations for small negatively charged water clusters indicate that the correlation energy associated with the unpaired electron is significantly smaller than that for valence electrons. This observation is in accord with such a simple model.[21] This independence also leads to structural properties which are somewhat similar to those of solvated anions.[22,23]

Heterogeneous hydrated electron systems have also been known and studied for some time. These systems, which may contain interfacial electrons, include excess electrons at aqueous interfaces of infinite size and negatively charged water clusters.[24] In water cluster anions, calculations clearly indicate that the excess electron can stabilize in two localization modes.[13,25,26,27,28,29] In interior-bound states the electron is localized in the interior of the cluster, surrounded by properly oriented solvent molecules. This system may be seen as the cluster analog of the bulk hydrated electron. A different molecular arrangement, which creates a substantial solvent dipole moment in the cluster, can stabilize the excess electron outside the molecular frame. The excess electron states in this case localize on the surface of the cluster. These water cluster anions are thus potentially analogous to excess electron states formed at a macroscopic interface.

Alternative assignments of experimentally observed data to IB or SB cluster anions[30,31,32] highlight the fact that the localization of the excess electron is a complex issue depending on the cluster size, the internal energy of the cluster, and possibly the cluster history. A recent simulation study indicated that the IB and SB cluster anions manifest individual patterns of cluster observable properties.[28,29] Based on the qualitative match between observed[33,34] and simulated optical absorption spectra, and the trends with increasing cluster size of the radius of the electron distribution and of the kinetic energy of the excess electron, it was concluded that the simulated properties of cluster anions with SB electron states correspond well to the experimental data.[28] Furthermore, in a subsequent study we pointed out that the interaction of neutral water clusters and slow electrons (the usual condition in cluster anion experiments) leads initially to surface electronic states. These non-relaxed cluster anions can be assumed to be the precursor states for the fully relaxed anionic species.[35]

The existence of the two types of water cluster anion isomers with significantly different physical properties offers potentially interesting links to infinite bulk and interfacially hydrated electron systems. The apparent differences in the behavior of the excess electron on surfaces and in bulk motivate the present study. An additional connection with excess electrons on ice/air interfaces may also become evident in low energy electron diffraction experiments on ice surfaces.[36] In the present study, we explore the physical properties of excess electrons at interfaces of different water phases with air. The main issue we address is the relaxation associated with localization of a ground state excess electron at the water/air interface. In particular, we investigate whether there are conditions (i.e., temperature) under which the electron persists in a surface state, and how the manipulation of the temperature may lead to the migration of the electron into the bulk. To cover a wide range of physically possible states, we perform our investigation on four distinct interfacial systems. We study and compare the relaxation of an excess electron at a) an ambient liquid water/air interface (T=300 K), b) a supercooled liquid water/air interface (T=200 K)[37], c) *Ih* ice/air surface (T=200 K) and d) amorphous solid water/air surface (T=100 K).

Relatively recently, two theoretical studies have been carried out along similar lines. Rodriguez and Laria have simulated an excess electron at a liquid water/air interface constraining the system to surface states at 300 K using a path-integral molecular dynamics method.[38] This work assumes that SB electrons relax to the bulk, and inspects the properties of a hypothetical, relaxed SB electron state. Baletto *et al*. carried out ab initio molecular dynamics simulation for an excess electron at a 200 K *Ih* ice/air surface.[39] Such a simulation includes a somewhat limited size (32 water molecules) and simulation time (for about 5 ps); we perform similar simulations for significantly larger systems for longer simulation time, at the price of using a more approximate computational model. The present simulations provide detailed molecular insight into the mechanism of the relaxation process.

The structure of the paper is the following. In Sec. II, we give the details of the simulation procedure with emphasis on the approximations used, and their applicability for the electron solvation problem. In Sec. III, the results of the simulations are given and analyzed for all four investigated interfacial systems. The discussion focuses on the structural and energetic aspects underlying the relaxation process, and a comparison of the four cases. Sec. IV summarizes the conclusions of the paper.

II. Methods

We performed mixed quantum-classical molecular dynamics (QCMD) simulations to investigate the relaxation of an excess electron in its ground state at four different water/air interface systems in the microcanonical (constant NVE) ensemble. Since the QCMD simulation technique applied here has been described in the literature,[40] we review only the most important features of the method. In the simulations, the water molecules are treated classically interacting via a simple, three-site potential (SPC) with internal flexibility,[41] while the excess electron is described by a quantum mechanical wave function. The interaction of the electron and the water molecules is modeled by an approximate pseudopotential.[19,42] The excess electron wave function is represented in plane-wave basis. The Schrödinger equation for the excess electron in the field of the classical water molecules is solved using an iterative and block Lanczos procedure.[40] The water molecules evolve under the combined influence of the other classical molecules and the electron (using the Hellman-Feynman force). The nuclear evolution is adiabatic during the dynamics, with the electron confined to remain in its ground state. The equations of motion for the nuclear evolution are integrated by the Verlet algorithm using a 1 fs timestep.[43]

The simulations at the aqueous interfaces were carried out in slab geometries. The slabs contained 1600 water molecules in all four investigated cases. For the liquid water and amorphous solid simulations, the dimensions of the simulation cell were chosen to be identical to that of bulk hydrated electron simulations in the *x*- and *y*-directions (36.34 Å) and four times this length perpendicular to the interface (*z*-direction).[19] For the ice *Ih* simulation the *x*- and *y*-dimensions were slightly different due to the hexagonal geometry (36.14 Å and 39.13 Å). The length of the cell in the *z*-direction extended to four times the length in the *x*-direction. The simulation cells were repeated periodically in three directions, so that the water slabs are separated by approximately 100 Å wide vacuum. The initial slab configurations for the liquid water simulation were taken from corresponding bulk simulations.[19] Cold amorphous structures were also generated from liquid configurations (see below). The ice *Ih* was constructed with 80 (40+40) molecules arranged in each of 20 bilayers in hexagonal structure with the (0001) surface in the *z*-direction. The proton arrangement was disordered, and satisfied the Bernal-Fowler ice rule. The ice slab had a vanishing dipole moment in the initial configuration.[44]

First, we carried out localization site analysis on the neutral interfaces similar to that we performed for neutral water clusters in a previous study.[35] The neutral liquid water slabs were equilibrated at the nominal temperatures 200 K and 300 K. The temperatures of the *Ih* ice and the amorphous ice structures were set to 200 K and 100 K, respectively. For the 200 K and the 300 K systems, we launched 200 ps long equilibrium trajectories, of which 499 configurations, 400 fs apart, were selected for the analysis. The configurations of the 100 K amorphous slab were generated starting from the selected neutral configurations at 300 K. The temperature of these configurations was reduced gradually to 100 K during a shorter 3 ps classical molecular dynamics run. We used the final configuration of each of these trajectories in the localization site analysis of the amorphous interface. The interaction energies between

the electron and the selected neutral slab configurations were calculated within the pseudopotential approach. The electron was represented on 32^3 evenly distributed grid points in a cubic box with side length equal to the shortest side length of the simulation box.

In a second step, we investigated the relaxation dynamics of the aqueous interfacial systems after adding an excess electron to the neutral slabs. For the 200 K and the 300 K liquid water/air interfaces, we ran 10-10 relaxation trajectories starting from randomly selected configurations of the long equilibrium neutral trajectories. The trajectories were run for 10 ps each, significantly longer than the longest relaxation timescales in ambient bulk hydrated electron systems. For comparison, we also examined the relaxation dynamics for the *Ih* ice/air interface and an excess electron, running only two trajectories, starting from different configurations. Besides the last configuration of the 200 ps long neutral equilibrium trajectory, an alternative *Ih* ice structure was generated for comparative purpose, by performing a Maxwell-Boltzmann velocity scaling scheme for only 1 ps starting from the original proton disordered ice structure, and taking the last configuration of the run. The two *Ih* ice/air interface trajectories with an excess electron were run for 180 ps and 120 ps, respectively, including the dynamics of all the molecules of the slab. We also performed a similar MD run (200 ps) for the relaxation of an excess electron on the 100 K amorphous solid interface starting from the most stable initial configuration of the localization analysis.

Since the electron quickly localizes during the relaxation trajectories (see discussion below), we represent the excess electron on a 32^3 grid only in the first 500 fs of the runs. Later times employ a smaller cubic grid box with 16^3 grid points and half the side length of the original. In order to follow the position of the electron distribution correctly during the nuclear evolution, the grid box was always centred at the centre of mass of the electron. Thus, the Schrödinger equation for the electron was solved in every nuclear propagation step twice:

first, on the grid at the previous nuclear configuration, and then, repeated on a (possibly) shifted grid centred on the newly computed electron distribution.

Before proceeding to the numerical results of the simulations, it is instructive to discuss the reliability of the potential energy calculations within the present QCMD approach for the electron solvation problem. Although the SPC water potential does not, in general, reproduce precise energetics, it is known to fare qualitatively well for various properties of liquid water, and we expect it to perform with similar adequate reliability for the investigated liquid and solid phases. The electron-water molecule pseudopotential, which has been parameterized with the flexible SPC model, is a key component of the algorithm. The present pseudopotential has predicted reasonably both the energetics and the spectroscopic properties of an equilibrium ground state hydrated electron.[19] Other successful applications are also documented.[45,46] Nevertheless, it has become clear, that the pseudopotential mainly neglects electron-molecule dispersion interactions.[25,26,27,47] Thus, one might anticipate that the regime involving small electron-cluster interaction energies is somewhat distorted by the present pseudopotential, being too weakly bound. In fact, a comparison of the energetics of small surface-bound water cluster anions using the pseudopotential approach and correlated ab intio MP2/6-31(1+3+)G* method[48] showed that the pseudopotential systematically underestimates the MP2 interaction energies by about 0.2 eV in the weakest interaction regime (the 30-400 meV interaction energy range with the pseudopotential). Nevertheless, the correlation between the interaction energies computed by the two methods is quite reliable.[35] Fully relaxed water cluster anions (n~45-200) were also examined very productively with the same pseudopotential.[28] The results for surface state anions showed underestimation of the experimental vertical detachment energies (VDE), but the qualitative trends for the computed VDEs and optical absorption spectra were in reasonably good agreement with experiments.[28]

This information taken together indicates that the pseudopotential-based method can be used with confidence in a wide range of stabilization energies for qualitative purposes.

III. Results and Discussion

Excess electron localization sites on the neutral interfaces

In the first step we investigate the initial localization sites of the excess electron on the neutral interfaces. These sites can serve as starting points for the ensuing relaxation dynamics. We analyzed the interaction of an excess electron with 499 equilibrium slab configurations for each interfacial system. The position of the electron relative to the water films is monitored by the distance between the center of mass of the electron and the center of mass of the slab in the z direction (perpendicular to the interface), $r = \left| z_{com,e} - z_{com,slab} \right|$. We compare r to the distance R between the Gibbs dividing surface[49] and the center of mass of the slab in the z direction, where $R = \left| z_{Gibbs} - z_{com,slab} \right|$. Surface-bound excess electrons are defined, as $r + r_e \geq R$ (or alternatively, $d = r + r_e - R \geq 0$), where r_e is the radius of gyration of the excess electron distribution. One can similarly identify interior states with $r + r_e \leq R$. We find that almost all slab configurations initially localize the electron in surface states outside the water slabs. Since only 0.1 % of all the configurations (2 cases) stabilize the electron in interior states, we neglect these cases in the analysis.

Similarly to previous work[35] we consider the electron physically localized in the field of the slab only if its radius of gyration is less than a predefined cutoff distance, $r_{cut} = \sqrt{\frac{3}{5}} \frac{l_{box}}{2}$, where l_{box} is the length of the cubic grid box used to represent the electron. According to this criterion, a significant fraction of the configurations localize the electron initially. The localized configurations make up approximately 45 % and 75 % of the

configurations on supercooled and ambient liquid water films, and 60 % and 75 % on amorphous solid layers at 100 K, and on *Ih* ice slabs at 200 K, respectively. The localization sites are always associated with the relative proximity of the electron to one or more dangling OH bonds on the surface. The initial stabilization energy of the localized excess electron is weak in all cases. A significant portion of the localized configurations are calculated to have slightly positive energies. This artifact is almost certainly due to the constraint of a relatively small grid size ($r_{cut} \approx 14$ Å) applied for the representation of the electron. In the slab geometry, the grid box size is determined by the smallest dimension of the simulation box. The value here is roughly half the size of that we used for finite size clusters.[35] These positive energy cases are therefore also probably very weakly stabilized, but the finite basis effect and the underestimation of the energy by our pseudopotential method would likely distort their properties in the analysis.

We show in Figure 1 the ground state energy distribution only for those configurations which satisfy both the geometric ($r_e<r_{cut}$) and energetic localization criteria ($E_0<0$ eV). Clearly, the excess electron stabilization is somewhat weaker on these neutral interfaces than in finite clusters.[35] We have also shown that the configurations with localized excess electron distribution for $(H_2O)_n$ neutral water clusters constitute 50 % of the total sample for n=20, with the localized fraction rapidly increasing with the cluster size; from n=104, practically all configurations support localized excess electron distribution.[35] The excess electron is stabilized on the interface initially by the electric field of the instantaneous dipole moment. Since the dipole moment vector of the slab is not necessarily perpendicular to the infinite surface, the effective instantaneous dipole moment felt by the electron on the surface may be significantly smaller than in the clusters, where the electron localizes predominantly in the direction of the dipole vector.[35] Nevertheless, the energy distributions of the slab configurations show sizeable initial stabilization for the excess electron up to -0.4 eV. As a

general trend, one observes that the average initial stabilization increases with the temperature. The size distributions of the electron also reflect these trends (Figure 2). The typical radius of gyration is around 6-10 Å, indicating a very diffuse electron distribution even for the localizing slab configurations. Nevertheless, what is most striking is that the distributions are very similar to one another.

Relaxation on the water/air interfaces

The initial localization of the excess electron is followed by substantial relaxation, in which the electron and the condensed phase mutually interact, and both relax. We investigate the simplest scenario here, and assume that the excess electron attached to the interface relaxes adiabatically on the ground state potential surface during the dynamics. The starting points used for the relaxation are randomly selected from the long equilibrium neutral trajectories.

We follow the details of the electron hydration dynamics by monitoring energetic and structural properties of the excess electron. Figure 3 shows the time evolution of the energy of the electron, the size of the electron distribution, and the distance of the center of mass of the electron to the Gibbs dividing surface ($r - R = z_{com,e} - z_{Gibbs}$) of two characteristic trajectories at T=200 K and T=300 K. These trajectories highlight the major difference in the relaxation channels at different temperatures. The relaxation always starts from very weakly bound, diffuse surface electron states. An ultrafast component of the hydration takes place within the first ~20 fs. This timescale corresponds well to the rotational motion of the dangling hydrogens around the hydrogen-bonded OH bonds. After ~100 fs the energy drops by roughly 0.5 eV and 2.0 eV for the two selected trajectories (see the inset in the top panel of Figure 3), and by about 0.5 eV and 1.0 eV in average for the 10 relaxation trajectories at 200 K and 300 K, respectively. The ultrafast stabilization leads to much more compact surface states; the size

of the electron typically collapses from the initial 8-10 Å to approximately 4 Å at 200 K, and 3 Å at 300 K, and the center of the electron quickly approaches the Gibbs dividing surface. Evidently, the process is significantly more effective at higher temperature. The stabilization of the SB states are enhanced by the interaction of the excess electron and the dipole field of the water layer, as indicated by the initial large increase of the normal component of the dipole moment vector of the slab during the ultrafast regime (not shown). After the first 100 fs the electron hydration takes place on longer timescales. The major difference in the dynamics at the two different temperatures becomes evident in the 1-10 ps range. In particular, one observes that at the lower temperature the SB excess electron state persists over the simulated timescale ($r + r_e - R \sim 0$), while the surface state transforms to an interior state in the 300 K trajectory ($r + r_e << R$). On the selected 300 K trajectory, this transition is evident at around 7 ps, as the electron gradually approaches the center of the slab (see the bottom panel of Figure 3). We have found that six of the 10 trajectories ended up in IB state at 300 K within the simulated 10 ps, while all trajectories remained in surface states at 200 K. Extension of the simulation timescale for those four 300 K trajectories which stayed in surface states after 10 ps resulted in interior states within approximately 40 ps. We have also chosen a single 200 K trajectory and extended the simulation for a relatively long 180 ps period. This trajectory has persisted in a surface state within the examined timeframe. We will return to the analysis of this single trajectory below.

The time dependent averages computed from the set of 10 relaxation trajectories provide additional insight in the relaxation phenomenon. The trajectory averages of the ground state energy of the excess electron and the energy gap between the ground state and the first excited state are shown in Figure 4. The general non-exponential character of the two curves is similar, but the longer time values are notably different at the two temperatures. The ground state energy of the excess electron approaches 2.0 eV at 200 K and 3.0 eV at 300 K

after 10 ps. A similarly large difference appears for the first electronic excitation gap; it is around 1.0 eV at 200 K, 1.5 eV at 300 K after 10 ps of relaxation. These large differences are due to two facts: a) the relaxation, in general, is faster at higher temperature, and b) the 200 K data are solely averages of persisting SB states, while those at 300 K are averages of both IB states and SB states at the end of the relaxation trajectories. Since inspection of individual trajectories shows that the relaxation of neither the surface states nor the interior states is over by 10 ps, we can anticipate further decrease in the value of these properties. In fact, one can expect that the asymptotic physical observables at 300 K are those of the bulk hydrated electron. On the same line, a sufficiently long surface state trajectory (generated at a lower temperature) would be needed to estimate the properties of the fully relaxed *surface state* electron. Such a trajectory is presented in Figure 5. This single, constant energy, *NVE* trajectory has been run for a total length of 180 ps, and possesses an approximately 140 ps long stable plateau at approximately 200 K.[50] The excess electron occupies an SB state during the entire dynamics. The ground state energy distribution for the 40-180 ps range (not shown) is symmetric, approximately Gaussian, with an average of -2.6 eV. The persistence of the plateau suggests that the surface state is at least kinetically stable for this particular trajectory. Other characteristic properties are in accord with this observation. The electron distribution is compact; the size of the electron varies between 2.2 Å and 3.6 Å with a 2.7 Å average radius. We note that this value is significantly smaller than that predicted from a previous simulation study for an artificially constrained surface state electron at T=300 K (3.6 Å).[38] In the current work, the excess electron localizes at a surface position in the water layer which corresponds roughly to a density that is 90 % of the bulk value, near to the Gibbs surface.

It is also instructive to take a brief look at the excited states of the surface-bound excess electron. We find that similarly to the fully hydrated electron the quasi-degeneracy of the three *p*-type excited states remains on the water/air interface. The optical absorption

spectrum for the surface state electron based on the 200 K long plateau (computed from 800 equidistant configurations) is shown in Figure 6. The computed spectrum, similarly to that of the hydrated electron,[14,19] is dominated by three *s* to *p* transition. The absorption band is broad and asymmetric, with a maximum at around 1.5 eV.

All the computed data for the surface-bound electron states on the supercooled water/air interface are fully consistent with the trends of the surface-bound electron states of the negatively charged water clusters simulated in a previous study.[28] It was noted, in particular, that the physical properties of the SB states exhibit only weak temperature dependence. The experimental observables are, thus expected to be basically the same over a very wide range of accessible cluster temperatures. Based on this observation, one can directly compare the physical properties of the supercooled water/air interface to those of SB state cluster anions. It was found, for example, in agreement with experimental results,[34] that the size of the excess electrons in a surface-bound state gradually shrinks as the cluster grows.[28] Our present finding for the radius of the electron at the water/air interface, 2.7 Å, fits in that trend and provides a reasonable estimate for the infinite cluster limiting case (cf. Fig. 4, Ref. 28). The average ground state energy of the excess electron on the interface (-2.6 ± 0.1 eV) differs relatively little from the average electronic energy of the SB state clusters simulated and extrapolated to infinite cluster size (-3.0 ± 0.3 eV).[28,51] The position of the maximum of the calculated absorption spectrum of the interface (1.5 eV) also relates favorably to the SB cluster extrapolated value (1.7 ± 0.3 eV).[28,51]

We note here, that the bulk (IB) hydrated electron simulations at 300 K with the same model potential resulted in somewhat lower ground state energy (-3.1 eV), more compact electron distribution (r_e=2.4 Å), and a spectrum which reflects larger energy gaps (1.9 eV maximum),[19] than those of the SB state at the substantially colder, 200 K interface. The comparison of the observables is, however, not expected to lead to exact agreement due to the

significant temperature dependence of the IB electron state properties. It was observed for IB state cluster anions that decreasing temperature leads to gradually more compact, more stable excess electron ground state, and significantly blue-shifting absorption band.[28] Similar effects were observed in simulations for the bulk hydrated electron, with the same model used here, which qualitatively reproduced the experimental temperature dependence of the spectra in the bulk liquid phase.[46] This work found that the spectral shift is entirely due to the density change of the liquid that arises from thermal expansion at constant pressure. The present model also predicts that the density increases by ~3% in the supercooled liquid state relative to the ambient water. Recently, Bartels and his co-workers have used isochoric state pairs for water lying above and below the temperature of maximum density to show that the density dependence alone is not sufficient to fully describe the temperature dependence of the position and the shape of the absorption band.[52] Nevertheless, they have found a significant blue shift of the spectrum with decreasing temperature. One, thus, can expect that a bulk hydrated electron occupies an even more stable ground state, and its spectral maximum shifts to larger energies in a supercooled liquid environment relative to ambient conditions.

These tendencies predict considerable differences in the observables of an SB state electron and an IB state electron. The data reflect the distinct differences in the molecular environment in surface compared to interior states. Based on the computed energetic (and spectroscopic) differences, we anticipate that these relaxed states could be distinguished experimentally, limited by the stability of the supercooled liquid.

We now consider molecular characterization of the surface and interior electron solvation structures. First, we evaluate the number of molecules surrounding the excess electron within a given radius of its center of mass. The time evolution of the coordination number within 5 Å averaged for the set of 10 relaxation trajectories is shown in Figure 7 at 200 K and at 300 K. Initially (t=0), the diffuse electron has only 2-4 water molecules within

its 5 Å radius. This number quickly increases reaching an average of 8 at 200 K, and 13 at 300 K, by 10 ps. The coordination number around the equilibrium hydrated electron at 5 Å, which can be calculated from the bulk pair distribution functions,[19] is approximately 16. This is in accord with the previously noted fact that the 300 K solvation dynamics at the interface has not completely finished yet. The increase of the coordination number of the electron at 300 K (Figure 7) reveals that the transition from surface to interior state is, on average, a gradual process under ambient conditions.

The coordination number for an SB state electron can be estimated from the long 200 K trajectory (Figure 5). The computed coordination number is ~10, confirming the expectation of reduced coordination, although, the coordination number for the surface state is more than half that of the equilibrium IB state. The surface state electrons localize in a concave depression on the solvent surface. The shape is easily pictured by a simple two-dimensional representation (Figure 8a). The center of mass of the electron is the origin, and the points in the figure represent the normal direction *z*-coordinate of the solvent oxygen atoms as a function of their axial distance from the electron's center in the *xy*-plane. The figure visualizes that, although the electron density deeply penetrates in the slab, the water molecules do not approach the electron from the interface. Figure 8b presents a corresponding characteristic slab configuration with the corresponding electron density at the supercooled water/air interface.

Relaxation on the ice/air interfaces

In order to explore the effect of initial conditions, we generated two relaxation trajectories for the *Ih* ice/air interface. The two cases differ only in the length of an initial equilibration period of the neutral slab. In one case, an ideal ice slab was equilibrated at 200 K for only 1 ps, while in a second scenario, the equilibration period was significantly longer,

130 ps. The electron was then included, and the relaxation dynamics were launched from the last configurations of the equilibrated trajectories.

In the first case, the electron is placed on a more regular ice surface. Accordingly, the trajectory initially relaxes more slowly than the more equilibrated structure, with the excess electron persisting in a less compact, slowly relaxing outer surface state for about 50 ps, and becoming more localized and more tightly bound during an additional ~50 ps. Nevertheless this state is still clearly surface-bound. The trends of the ground state energy, the radius of gyration, and the normal component of the electron's center of mass distance to the Gibbs dividing surface all support this conclusion (not shown). Interestingly, the relaxation dynamics following the longer equilibration procedure essentially skips the more diffuse stage, and the electron very quickly localizes (within 1 ps) in substantially the same SB state. For later reference, we will denote this stable (or metastable) interfacial excess electron configuration state as surface structure I. A corresponding characteristic configuration of the water molecules and the associated electron density are shown in Figure 9. We note that in this particular configuration of structure I, one can visually identify four water molecules pointing with an OH bond toward the electron (upper panel). A more detailed structural analysis is given below.

The physical properties of this SB electron on the hexagonal ice/air interface is basically identical to those observed for the supercooled liquid water/air interface, with -2.7 eV ground state energy, and 2.6 Å radius. The ground state excitation energy distribution for surface structure I also resembles closely that for the supercooled water/air interface, with an apparent slight, 0.1 eV, blue-shift, with a maximum at around 1.6 eV. These data all suggest that the excess electron at the ice surface behaves quite similarly to the surface of supercooled water. This conclusion is consistent with the report of Wei *et al.* that a disordered liquid-like layer is formed on the ice surface beginning at around 200 K.[53]

Simulations for the 100 K amorphous solid water complement the picture. Figure 10 shows the time evolution of the most important physical properties along a relaxation trajectory of an excess electron, initially placed on the surface of a neutral amorphous solid slab. The electron localizes very quickly, its radius collapsing from 11 Å to 5 Å within the first 20 fs (not resolved on the figure). Nevertheless, the energy drops only ~0.2 eV, due to the rigidity of the water structure. Correspondingly, the subsequent relaxation is a slow process relative to the higher temperature cases. A sudden energy drop after about 150 ps, yields an apparently kinetically stable species with a ground state energy averaging about -1.6 eV. Although this state is also an SB state, it is significantly higher in energy and more diffuse (~3 Å radius) than surface structure I. Due to its distinct characteristics, we denote this state as surface structure II.

Now we consider structural characterization of surface structures I and II based on the hydrogen-bonding properties of the water/air and ice/air interfaces with the excess electron. In particular, we examine whether our simulations predict the unique, double hydrogen-bonding acceptor (AA) binding site observed by Johnson and coworkers in vibrational predissociation spectroscopy measurements on small water cluster anions.[54,55] In the analysis, we evaluate the hydrogen-bonding properties of the water molecules to other water molecules in the vicinity of the electron. We define two water molecules as hydrogen-bonded if the intermolecular oxygen-hydrogen distance is shorter than 2.4 Å, and the corresponding O…O-H angle is less than 45º. A single water molecule can have two donor and two acceptor sites. The majority of the water molecules fall in the four hydrogen-bond, double acceptor – double donor, case (AADD). Of the several other patterns, the water molecules which play a crucial role in the stabilization of the excess electron are those with one or two hydrogen atoms that are not involved in H-bonds with other water molecules. The relevant cases are, thus, the double acceptor water molecules (AA) with two free hydrogen atoms, and the double acceptor –

single donor molecules with one unbound hydrogen atom (AAD). Figure 11 shows the number of AA, AAD and AADD water molecules as a function of the electron-oxygen distance for structure I of the *Ih* ice interface (200 K), and for structure II of the amorphous solid water interface (100 K).[56] The hydrogen bonding patterns show distinct differences between structures I and II. Most importantly, water molecules of AA type are located nearest the electron in structure I, in an average ~3 Å electron-oxygen distance (top panel of Figure 11). Within 5 Å distance to the electron, we find on average approximately three AA water molecules. Their orientation is predominantly hydrogen bond directed (not shown), but both hydrogen atoms are sufficiently near to the electron to interact with its wave function. Water molecules with one free hydrogen atom (AAD) also participate in stabilizing interfacial electrons, although they appear slightly farther from the electron than the AA molecules. As a characteristic difference, AA type water molecules do *not* appear in the local hydrogen-bonding pattern of structure II; only double acceptor – single donor (AAD) water molecules participate in stabilizing the interfacial electrons (see bottom panel, Figure 11). This observation clearly points to a structural aspect of the interfacial hydrogen-bonding structure, which is primarily responsible for the approximately 1 eV difference in the stabilization energy of the electron in structures I and II. For comparison, Figure 11 also shows the number of AADD type water molecules. The AADD motif, characteristic of the bulk, appears farther from the electron than the AA or AAD patterns, and its number grows very quickly. These molecules mainly donate hydrogen-bond(s) to the interfacial AA, and AAD molecules. Within 5 Å distance to the electron, no other hydrogen-bonding motif is present. Local hydrogen-bonding analysis for the supercooled liquid/air interface (not shown) predicts identical patterns as seen for structure I with AA hydrogen-bonding water molecules dominating in the electron-water interaction. This fact further supports that the relaxed

structure of the hexagonal ice/air interface is practically identical to that of the supercooled liquid water/air interface.

IV. Conclusions

We have examined the relaxation dynamics of excess electrons on interfaces of various water phases with air. The investigated phases included ambient water/air, supercooled water/air, *Ih* ice/air and amorphous solid water/air interfaces. We found that the starting point of the dynamics in all cases is the localization of an excess electron at the surface of the condensed phase. The excess electron initially occupies a diffuse, weakly bound state, and is stabilized by the dipole moment of the liquid layer. At the beginning of the relaxation, within the first 20 fs, the electron collapses and stabilizes on the surface. This part of the dynamics corresponds well to the timescale of rotational degrees of freedom, in particular, the rotational motion of the free OH bonds. The following relaxation strongly depends on the temperature, although the main stages of the process are common for all systems. For the 300 K liquid water/air interface, we observe that the excess electron gradually stabilizes, and eventually diffuses into the bulk. The transition of the electron from surface-bound state to interior-bound state takes place in the 10 ps timescale. This result indicates that under ambient conditions the excess electron is stable in interior state. Decreasing the temperature significantly slows down this process. In fact, on lower temperature interfaces, we did not observe transition to the IB state during the timeframe of the simulations. For the supercooled liquid/air interface the electron persists on the surface in a compact SB state in a deep, concave depression. Typically three AA water molecules stabilize this SB state, pointing their OH bonds toward the excess electron. It is especially noteworthy that the physical properties of the surface state electron (i.e. ground state energy,

size and absorption spectrum) in its long, stable (metastable) plateau for the supercooled water/air interface agree reasonably with the values extrapolated to infinite size for SB cluster anions in a previous simulation study.[28]

The more rigid structure of the solid phases relaxes more slowly, and the excess electron remains on the solid water/air interfaces during the dynamics. The relaxation dynamics exhibit distinct, clearly separated features depending on the temperature and the structure of the solid phases. These features are associated with well defined structural patterns, and thus, different types of surface states. The distinguishable SB structures are manifest in stable (metastable) plateaus of the trajectories, both in energy and geometry. The most stable *Ih* ice/air structure (structure I) has practically identical features to those for the SB electron at the supercooled water/air interface. The size, the ground state energy of the electron and the dominant hydrogen-bonding motifs near the electron indicate that a disordered liquid-like layer is formed on the ice, which, thus, behaves similarly to the supercooled liquid water/air interface. A typical, less stable and more diffuse SB state (structure II) is formed on the 100 K amorphous solid water/ice interface. The hydrogen-bonding network is significantly different from that of structure I. Structure II is characterized by the complete lack of AA type hydrogen-bonding water molecules, the dominant hydrogen-bonding motif on the interface being the AAD type pattern. Apparently, structure II is a metastable SB state, which may persist at low temperatures.

The present observations are consistent with the results of a previous simulation study on negatively charged water clusters.[28,29] We have shown that the simulated properties for the interfacial SB electrons at the supercooled water/air and *Ih* ice/air interfaces reasonably approach simulated cluster values extrapolated to infinite size.

Acknowledgment

L.T. gratefully acknowledges the tenure of the Bolyai Research Fellowship, and the Öveges Research Fellowship. The work was supported by a grant to L. T. from the National Research Fund of Hungary (OTKA) under Contract No. T049715. P. J. R. is grateful to the National Science Foundation (CHE-0615173) and the R. A. Welch Foundation (F-0019) for support of this work.

Figure Captions

Figure 1. The ground state energy distributions of the excess electron unrelaxed localization sites on liquid water/air (solid), supercooled liquid water/air (dashed), *Ih* ice/air (dotted), and amorphous solid water/air (dash-dot) interfaces for those configurations which satisfy both the geometric (r_e<r_{cut}) and energetic localization criteria (E_0<0 eV).

Figure 2. The radius of gyration distributions of the ground state excess electron on ambient liquid water/air (solid), supercooled liquid water/air (dashed), *Ih* ice/air (dotted), and amorphous solid water/air (dash-dot) interfaces for those configurations which satisfy both the geometric (r_e<r_{cut}) and energetic localization criteria (E_0<0 eV).

Figure 3. Time evolution of the ground state energy, the radius of gyration, and the normal distance of the center of mass of an excess electron to the Gibbs dividing surface at liquid water/air interfaces. A selected trajectory characteristic of 200 K (dashed), and a trajectory characteristic of 300 K (solid) are shown. The insets show the ultrafast part of the trajectories.

Figure 4. Trajectory averages for the ground state energy of the excess electron (top panel), and the energy gap between the ground state and the first excited state energies (bottom panel) at water/air interfaces at 200 K (dashed) and 300 K (solid).

Figure 5. Time evolution of the ground state energy of the excess electron in an SB state trajectory in the supercooled liquid water/air system (200 K).

Figure 6. Optical absorption spectrum of a surface bound excess electron at the supercooled (200 K) liquid water/air interface (solid). For comparison we show the spectrum calculated with the same model potential for the bulk hydrated electron at T=300 K (dashed).[19]

Figure 7. Coordination number for the ground state of the excess electron at water/air interfaces within 5 Å to the center of the electron distribution in supercooled (dashed) and ambient conditions (solid).

Figure 8. (a) The normal *z*-coordinate of the solvent oxygen as a function of their axial distance from the excess electron's center in the *xy*-plane at the supercooled 200 K liquid interface. (b) A characteristic configuration with the corresponding SB electron density. The isosurface contains 80 % of the electron distribution.

Figure 9. Characteristic slab configuration with the corresponding surface bound electron distribution for structure I of *Ih* ice/air interface at 200 K. The isosurface contains 80 % of the electron distribution.

Figure 10. Time evolution of the ground state energy, the radius of gyration, and the normal distance of the center of mass of an excess electron to the Gibbs dividing surface at an amorphous solid water/air interfaces at T=100 K.

Figure 11. Number of AA (solid), AAD (dashed) and AADD (dotted) types of hydrogen-bonding water molecules as a function of the distance of the oxygen atoms from the electron at *Ih* ice/air interface at 200 K (structure I, top panel), and amorphous solid water/air interface at 100 K (structure II, bottom panel).

Figure 1. Madarász, Rossky, and Túri

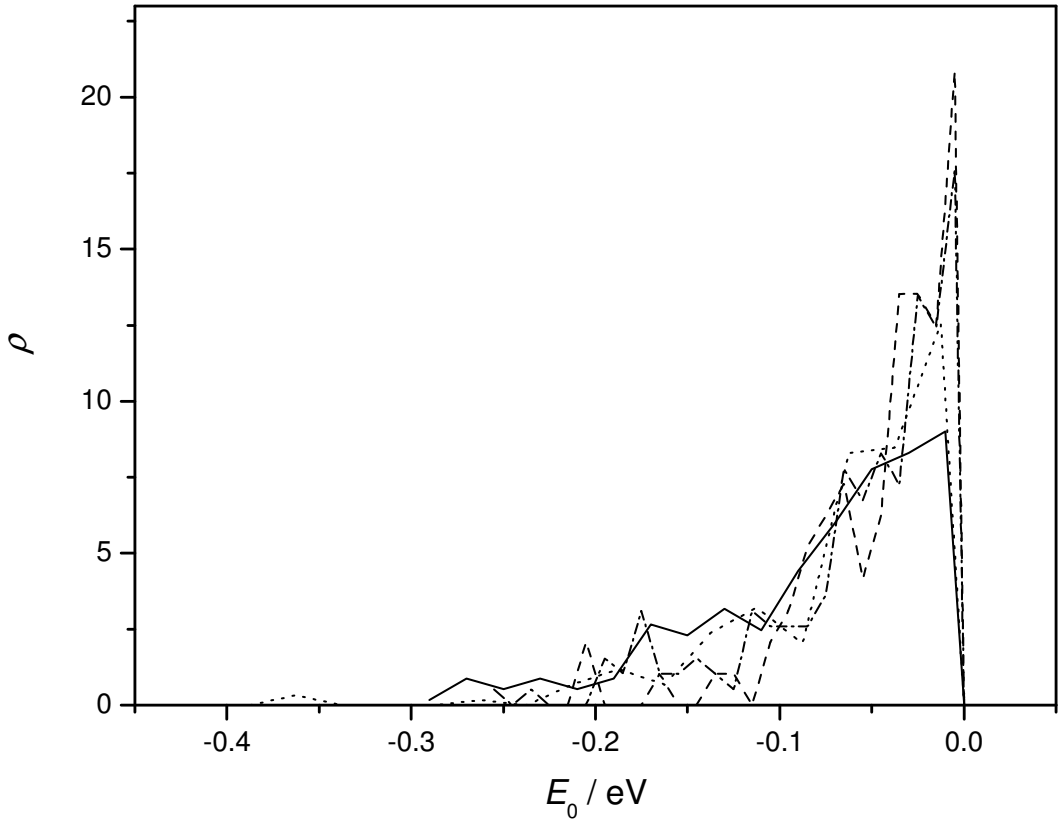

Figure 2. Madarász, Rossky, and Túri

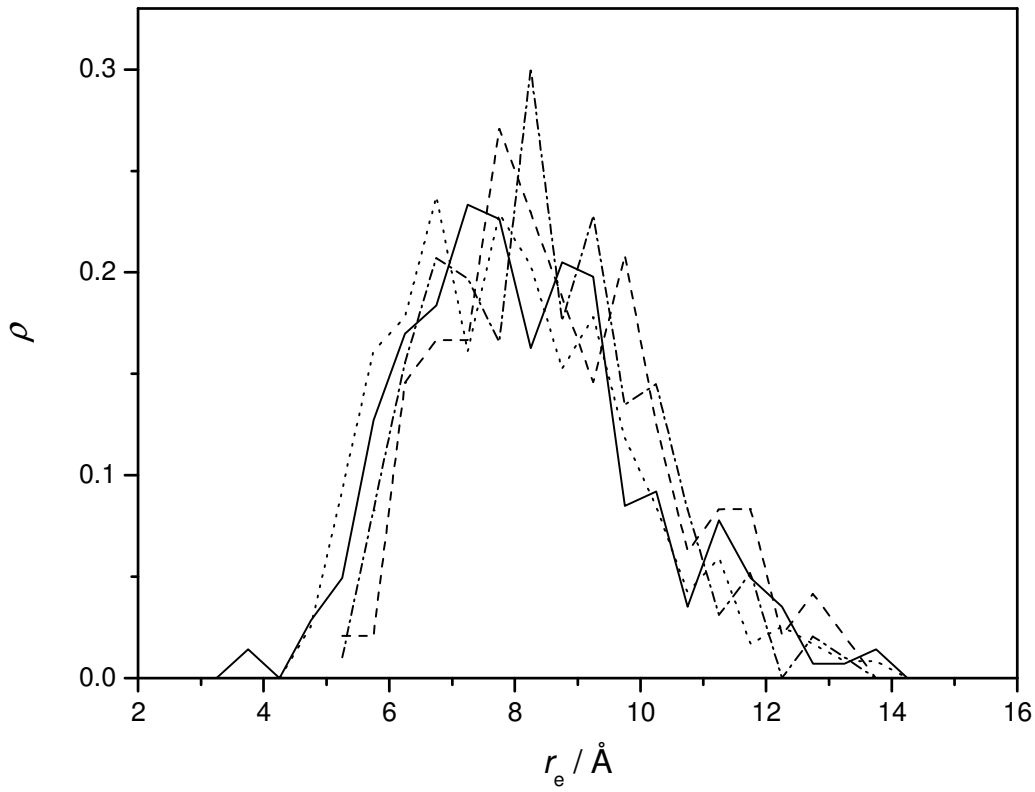

Figure 3. Madarász, Rossky, and Túri

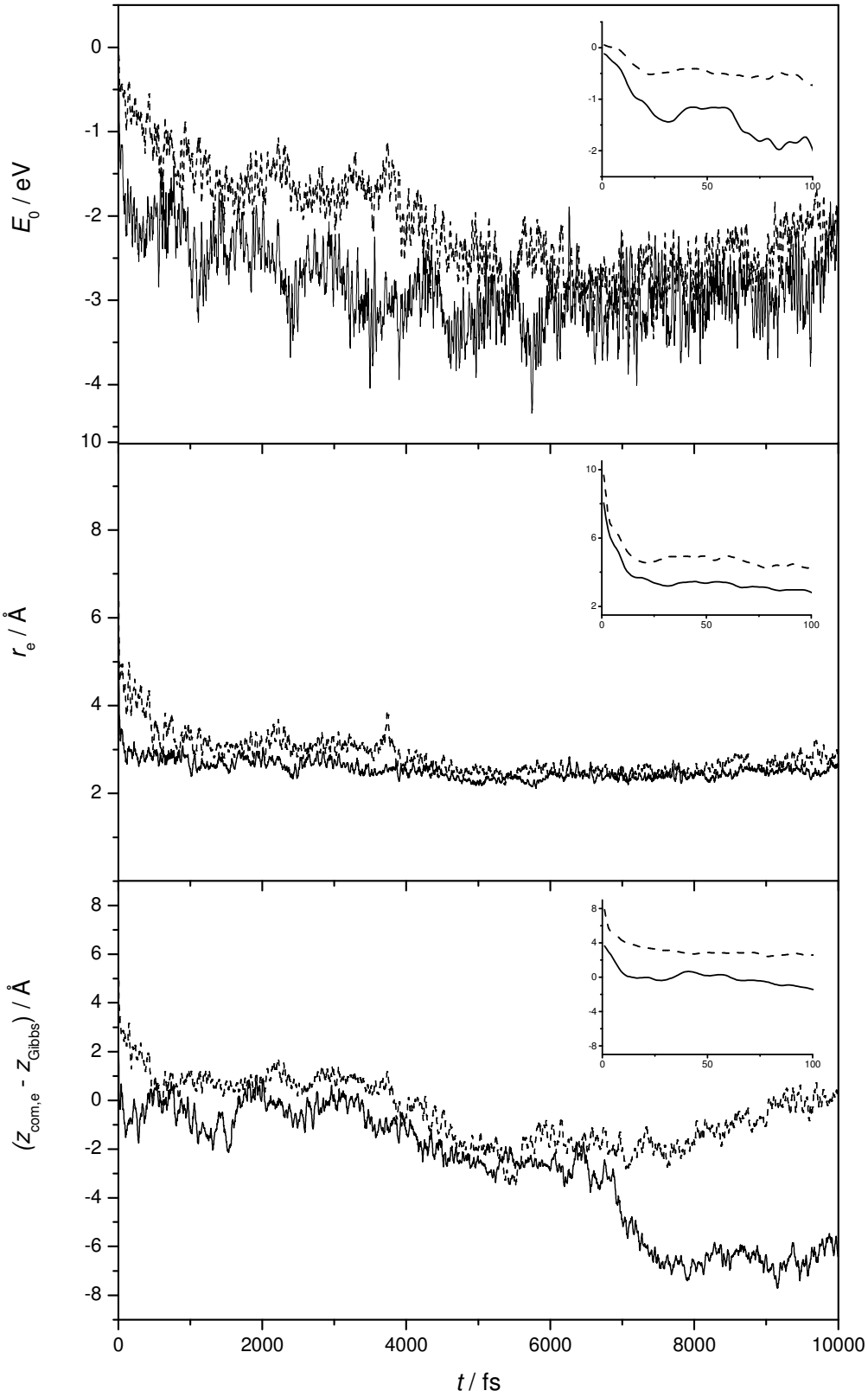

Figure 4. Madarász, Rossky, and Túri

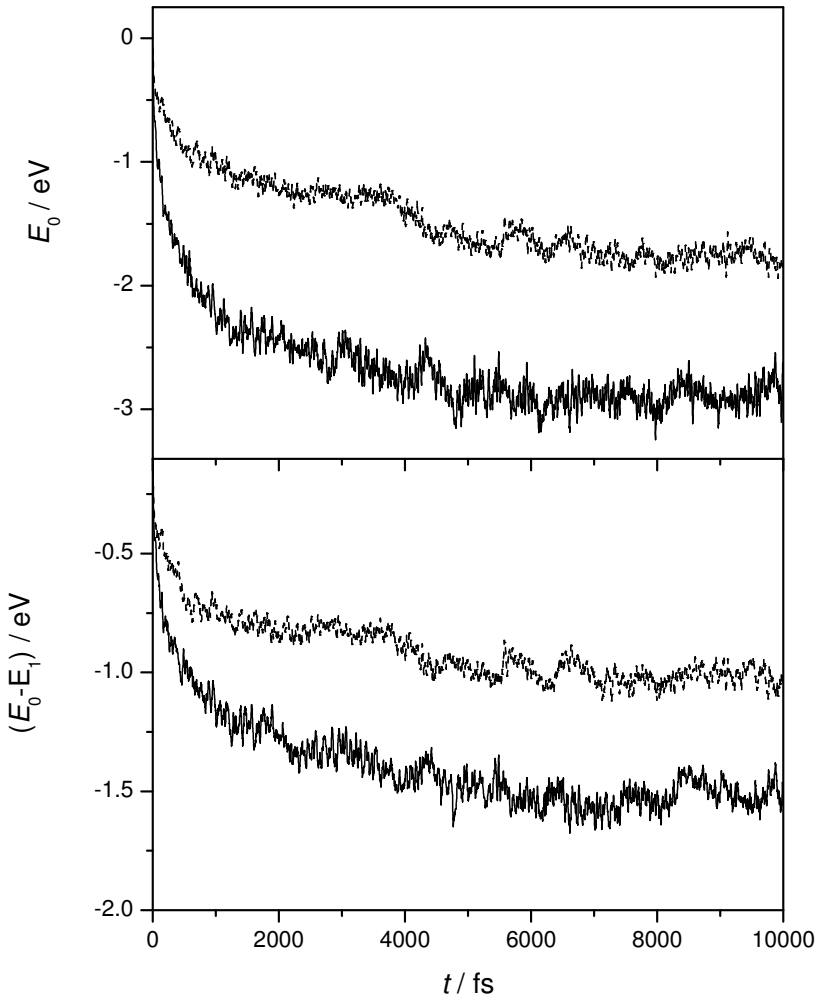

Figure 5. Madarász, Rossky, and Túri

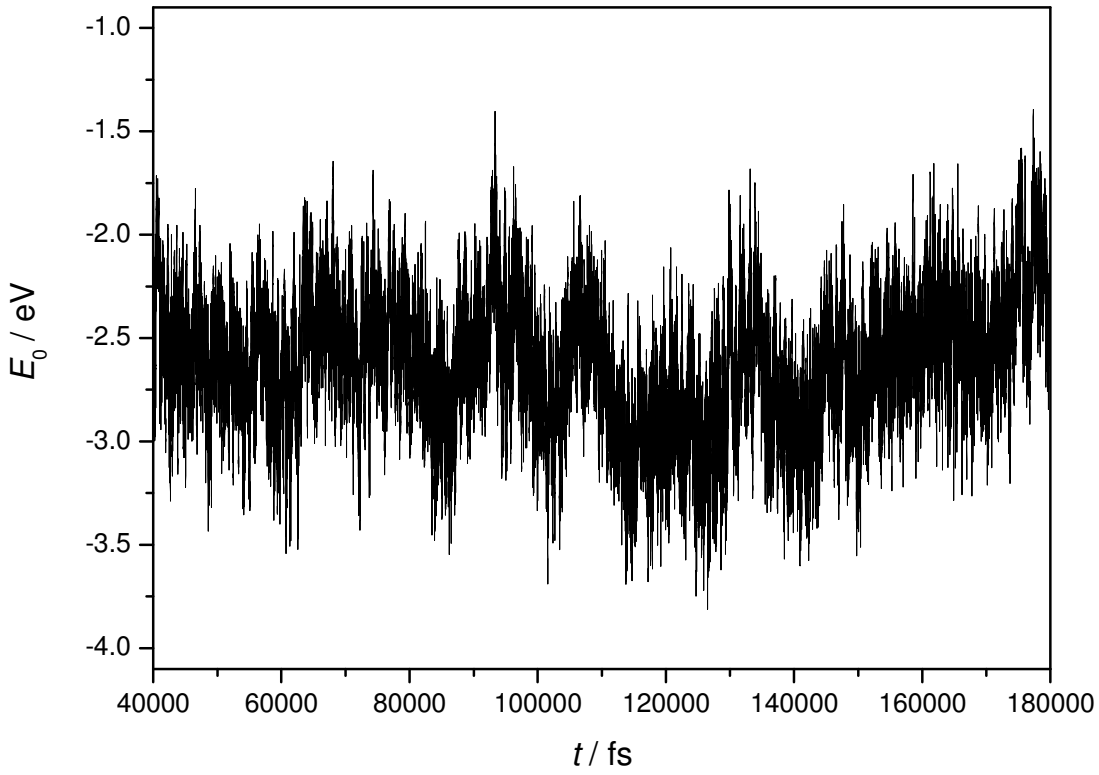

Figure 6. Madarász, Rossky, and Túri

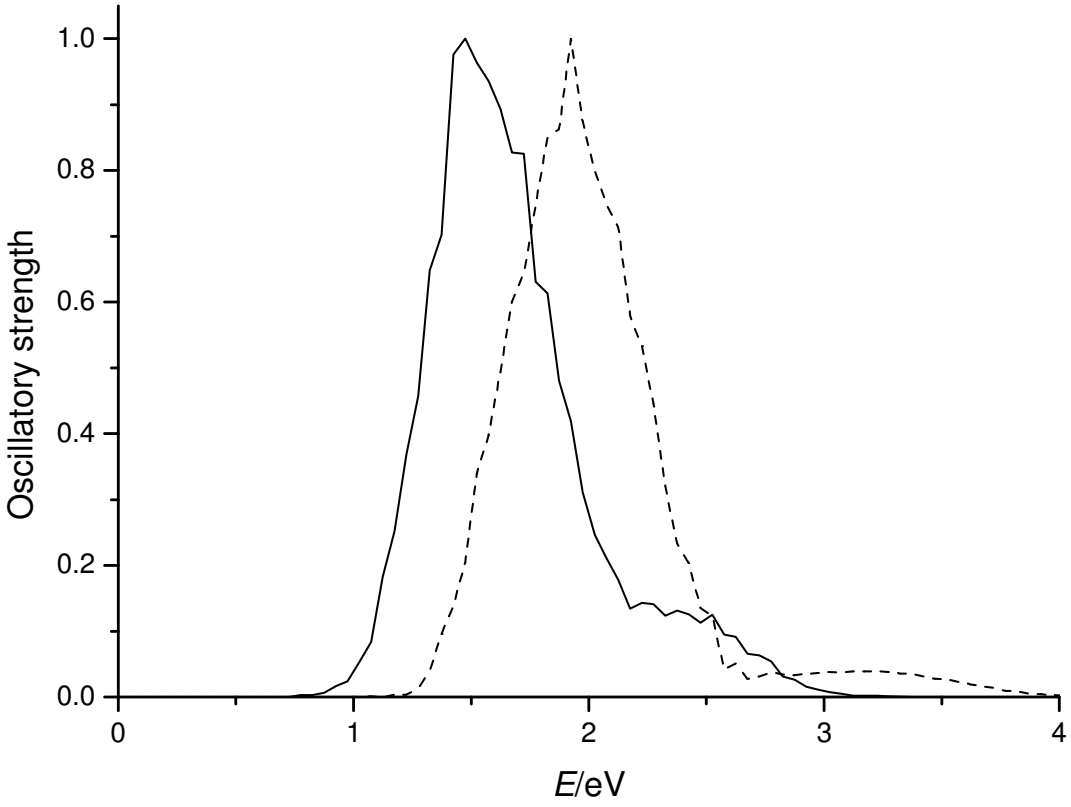

Figure 7. Madarász, Rossky, and Túri

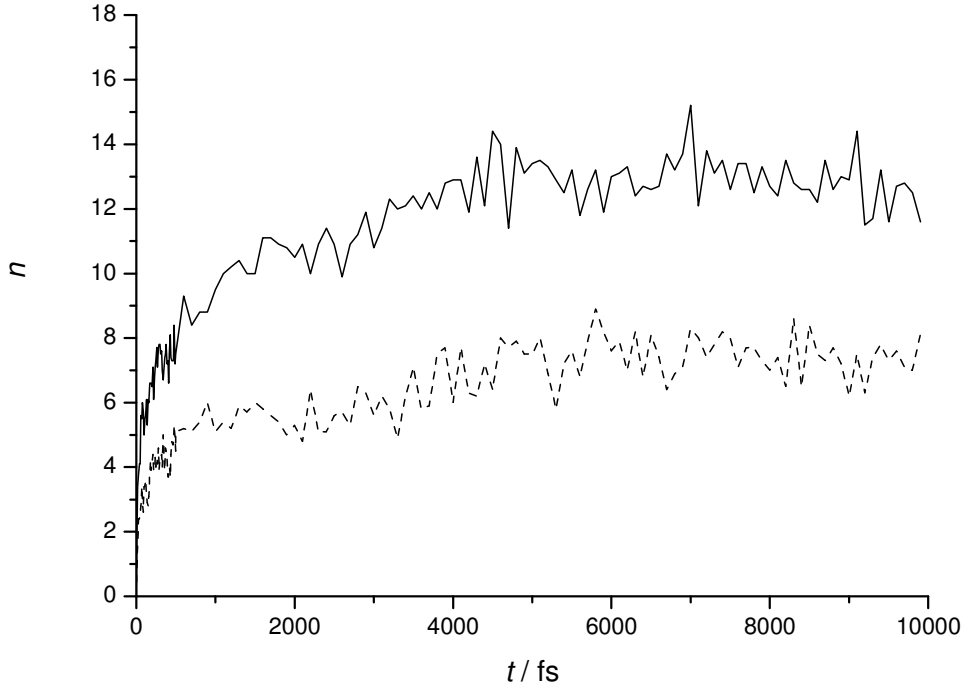

Figure 8. Madarász, Rossky, and Túri

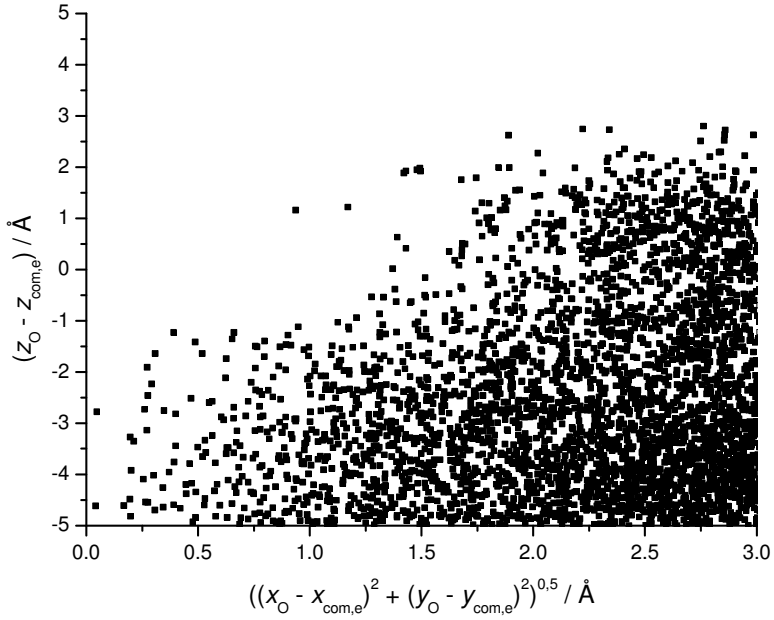

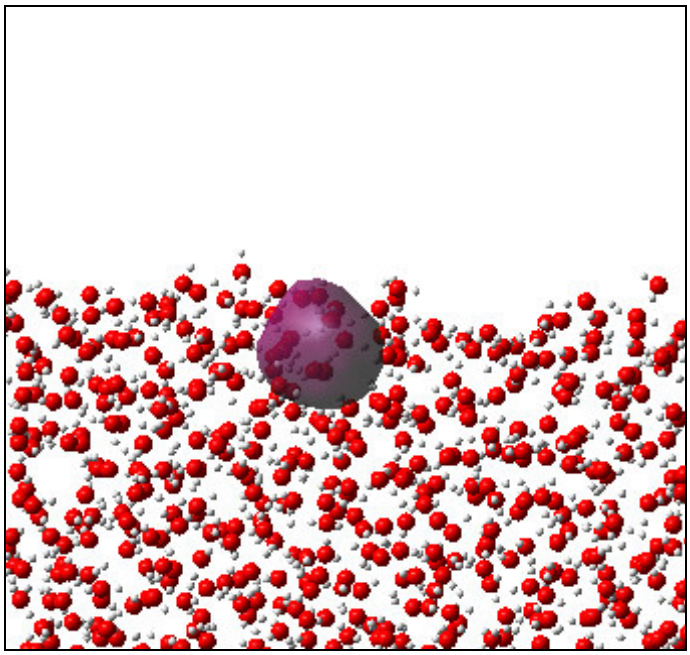

Figure 9. Madarász, Rossky, and Túri

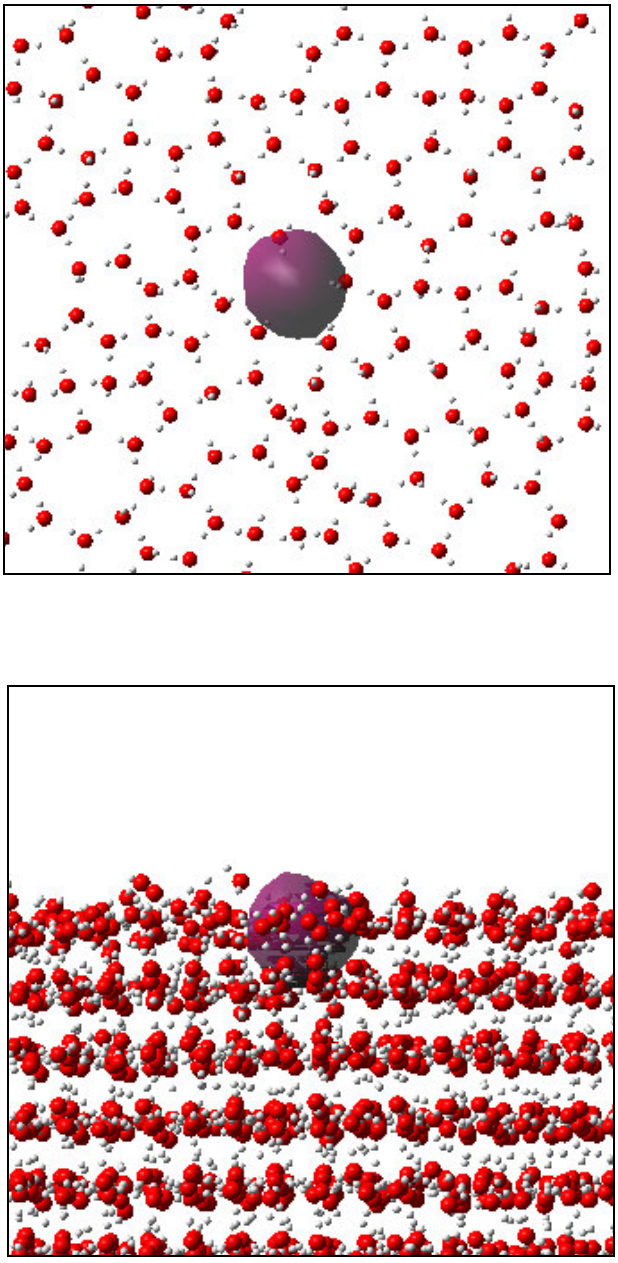

Figure 10. Madarász, Rossky, and Túri

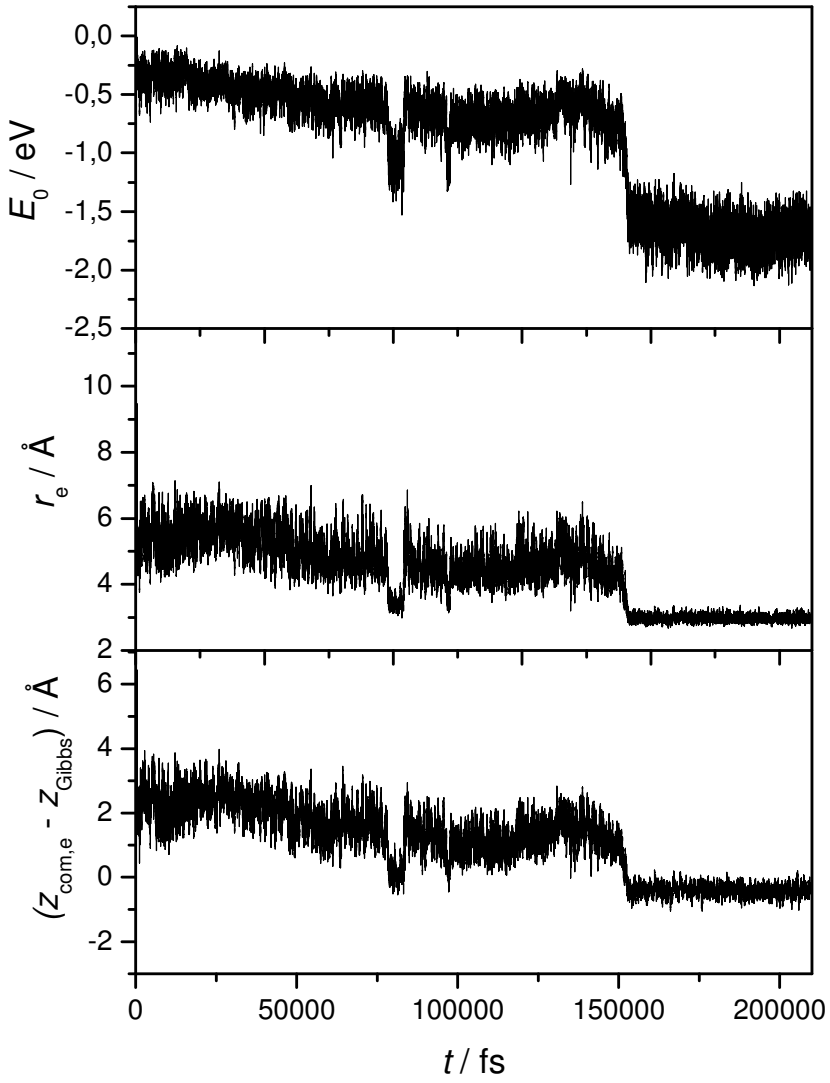

Figure 11. Madarász, Rossky, and Túri

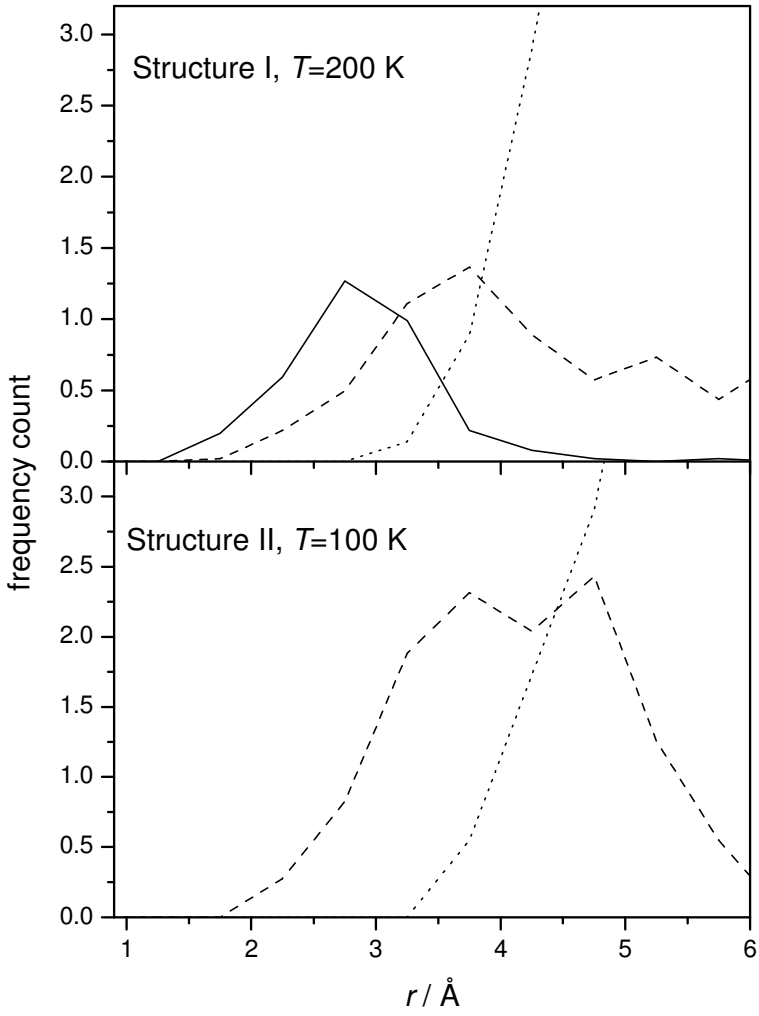

References

[1] C. Garrett, D. A. Dixon, D. M. Camaioni, D. M. Chipman, M. A. Johnson, C. D. Jonah, G. A. Kimmel, J. H. Miller, T. N. Rescigno, P. J. Rossky, S. S. Xantheas, S. D. Colson, A. H. Laufer, D. Ray, P. F. Barbara, D. M. Bartels, K. H. Becker, K. H. Bowen, Jr., S. E. Bradforth, I. Carmichael, J. V. Coe, L. R. Corrales, J. P. Cowin, M. Dupuis, K. B. Eisenthal, J. A. Franz, M. S. Gutowski, K. D. Jordan, B. D. Kay, J. A. LaVerne, S. V. Lymar, T. E. Madey, C. W. McCurdy, D. Meisel, S. Mukamel, A. R. Nilsson, T. M. Orlando, N. G. Petrik, S. M. Pimblott, J. R. Rustad, G. K. Schenter, S. J. Singer, A. Tokmakoff, L.-S. Wang, C. Wittig, and T. S. Zwier, Chem. Rev. **105**, 355 (2005).

[2] J. Zhao, B. Li, K. Onda, M. Feng, and H. Petek, Chem. Rev. **106**, 4402 (2006).

[3] C. A. Kraus, J. Am. Chem. Soc. **30**, 1323 (1908).

[4] E. J. Hart and J. W. Boag, J. Am. Chem. Soc. **84**, 4090 (1962).

[5] L. Kevan, Adv. Radiat. Chem. **4**, 181 (1974).

[6] A. Migus, Y. Gauduel, J. L. Martin, and A. Antonetti, Phys. Rev. Lett. **58**, 1559 (1987).

[7] F. H. Long, H. Lu, and K. B. Eisenthal, Phys. Rev. Lett. **64**, 1469 (1990).

[8] J. C. Alfano, P. K. Walhout, Y. Kimura, and P. F. Barbara, J. Chem. Phys. **98**, 5996 (1993)

[9] M. Assel, R. Laenen, and A. Laubereau, Chem. Phys. Lett. **317**, 13 (2000).

[10] T. W. Kee, D. H. Son, P. Kambhampati, and P. F. Barbara, J. Phys. Chem. A **105**, 8434 (2001).

[11] M. S. Pshenichnikov, A. Baltuska, and D. A. Wiersma, Chem. Phys. Lett. **389**, 171 (2004).

[12] A. Wallqvist, D. Thirumalai, and B. J. Berne, J. Chem. Phys. **86**, 6404 (1987).

[13] R. N. Barnett, U. Landman, C. L. Cleveland, and J. Jortner, J. Chem. Phys. **88**, 4429 (1988).

[14] J. Schnitker and P. J. Rossky, J. Chem. Phys. **86**, 3462 (1987).

[15] J. Schnitker, K. Motakabbir, P. J. Rossky, and R. Friesner, Phys. Rev. Lett. **60**, 456 (1988).

[16] E. Neria, A. Nitzan, R. N. Barnett, and U. Landman, Phys. Rev. Lett. **67**, 1011 (1991).

[17] B. J. Schwartz and P. J. Rossky, J. Chem. Phys. **101**, 6902 (1994).

[18] A. Staib and D. Borgis, J. Chem. Phys. **103**, 2642 (1995).

[19] L. Turi and D. Borgis, J. Chem. Phys. **117**, 6186 (2002).

[20] M. Boero, M. Parrinello, K. Terakura, T. Ikeshoji and C. C. Liew, Phys. Rev. Lett. **90**, 226403 (2003).

[21] J. M. Herbert, and M. Head-Gordon, Phys. Chem. Chem. Phys. **8**, 68 (2006).

[22] R. W. Impey, P. A. Madden, and I. R. McDonald, J. Phys. Chem. **87**, 5071 (1983).

[23] K. Heinzinger, Pure Appl. Chem. **57**, 1031 (1985).

[24] J. Zhao, B. Li, K. Onda, M. Feng, and H. Petek, Chem. Rev. **106**, 4402 (2006).

[25] K. D. Jordan, Science **306**, 618 (2004).

[26] T. Sommerfeld, and K. D. Jordan, J. Phys. Chem. A **109**, 11531 (2005)

[27] T. Sommerfeld, and K. D. Jordan, J. Am. Chem. Soc. **128**, 5828 (2006).

[28] L. Turi, W.-S. Sheu, and P. J. Rossky, Science **309**, 914 (2005).

[29] L. Turi, W.-S. Sheu, and P. J. Rossky, Science **310**, 1769 (2005).

[30] J. R. R. Verlet, A. E. Bragg, A. Kammrath, O. Cheshnovsky, and D. M. Neumark, Science **307**, 93 (2005).

[31] J. R. R. Verlet, A. E. Bragg, A. Kammrath, O. Cheshnovsky, and D. M. Neumark, Science **310**, 1769 (2005).

[32] J. V. Coe, S. T. Arnold, J. G. Eaton, G. H. Lee and K. H. Bowen, J. Chem. Phys. **125**, 014315 (2006).

[33] P. Ayotte, and M. A. Johnson, J. Chem. Phys. **106**, 811 (1997).

[34] D. M. Bartels, J. Chem. Phys. **115**, 4404 (2001).

[35] L. Turi, Á. Madarász, and P.J. Rossky, J. Chem. Phys. **125**, 014308 (2006).

[36] N. Materer, U. Starke, A. Barbieri, M. A. Van Hove, G. A. Somorjai, G.-J. Kroes, and C. Minot, J. Phys. Chem. **99**, 6267 (1995).

[37] The 200 K temperature liquid water corresponds to the supercooled state in the present classical model.

[38] J. Rodriguez, and D. Laria, J. Phys. Chem. B. **109**, 6473 (2005).

[39] F. Baletto, C. Cavazzoni, and S. Scandolo, Phys. Rev. Lett. 95, 176801 (2005).

[40] F. A. Webster, P. J. Rossky and R. A. Friesner, Comput. Phys. Commun. **63**, 494 (1991).

[41] K. Toukan, and A. Rahman, Phys. Rev. B **31**, 2643 (1985).

[42] L. Turi, M.-P. Gaigeot, N. Levy, and D. Borgis, J. Chem. Phys. **114**, 7805 (2001).

[43] M. P. Allen, and D. J. Tildesley, *Computer Simulation of Liquids* (Clarendon, Oxford, 1987).

[44] The geometry of the *Ih* ice structure was kindly provided by A. Bartók and G. Baranyai.

[45] R. Spezia, C. Nicolas, A. Boutin and R. Vuilleumier, Phys. Rev. Lett. 91, 208304 (2003).

[46] C. Nicolas, A. Boutin, B. Levy and D. Borgis, J. Chem. Phys. **118**, 9689 (2003).

[47] K. D. Jordan, and F. Wang, Ann. Rev. Phys. Chem. **54**, 367 (2003).

[48] J. M. Herbert, and M. Head-Gordon, J. Phys. Chem. A **109**, 5217 (2005).

[49] The Gibbs dividing surface is located at 16.0-16.7 Å distance from the center of the slab for the investigated systems. The dividing surface is placed to that surface position where the density is 90 % of the bulk average density.

[50] The average temperature of the plateau between 40 ps and 180 ps is 206 K.

[51] The error bars correspond to 95 % confidence intervals.

[52] Y. Du, E. Price, and D. Bartels, Chem. Phys. Lett., in press.
(doi: 10.1016/j.cplett.2007.03.027).

[53] X. Wei, P. B. Miranda, and Y. R. Shen, Phys. Rev. Lett. **86**, 1554 (2001).

[54] N. I. Hammer, J.-W. Shin, J. M. Headrick, E. G. Diken, J. R. Roscioli, G. H. Weddle, and M. A. Johnson, Science, **306**, 675 (2004).

[55] N. I. Hammer, J. R. Roscioli, J. C. Bopp, J. M. Headrick, and M. A. Johnson, J. Chem. Phys. **123**, 244311 (2005).

[56] In the analysis, we evaluated 101 configurations for structure I, and 51 configurations for structure II.